Sulfur Atoms Bridging Few-Layered MoS_2 with S-Doped Graphene Enable Highly Robust Anode for Lithium-Ion Batteries

*Xiaolei Wang, Ge Li, Min Ho Seo, Fathy M. Hassan, Md Ariful Hoque, and Zhongwei Chen**

Tremendous research interest from both academy and industry has been dedicated to the rechargeable lithium-ion batteries (LIBs) in the last decades for the upcoming era of portable electronics, electric vehicles (EVs), and hybrid electric vehicles (HEVs).[1–3] As one of the favorite power sources, most commercial LIBs utilize natural or synthetic graphite as the anode material due to its low cost, high Coulombic efficiency, and flat and low average potential of 0.2 V (vs Li/Li^+), as well as long cycle life.[4,5] However, its specific capacity of 372 mA h g^{-1} results in a device energy density of ≈150 W h kg^{-1}, which is much lower than that of internal-combustion engines and cannot meet the EVs requirements.[6] Therefore, there is an urgent need to develop novel anode materials with high theoretical capacities to replace graphite in next-generation high energy LIBs.[7–9] So far, various materials have been extensively studied for LIBs anodes,[10] including alloys (e.g., Si[11,12] and Sn[13]) and transition metal oxides[14] (e.g., $Li_4Ti_5O_{12}$[15,16] and SnO_2.[17,18] Although most of these materials possess a significant larger specific capacity, they suffer from either poor cycling life due to volume change associated with Li-ion insertion/extraction or sluggish electrode kinetics stemmed from slow ion diffusivity or intrinsic poor electron conductivity.[19] Compared to metal oxide materials, some transition metal sulfides possess high specific capacity and unique structures,[20] and have been considered as promising candidates for high-performance anode materials.

Among various candidates, a typical member of transition metal sulfide–molybdenum disulfide (MoS_2) possesses a similar layered structure to graphite but a much larger interlayer spacing of 6.15 Å (vs 3.35 Å of graphene) by stacking together through van der Waals interactions, which facilitates lithium-ion intercalation without a significant volume expansion.[21,22] However, MoS_2 still suffers from fast structural deterioration during lithiation/delithiation process and poor electrical/ionic conductivity, resulting in unsatisfactory cycling performance and rate capability in LIBs application. Current approaches for developing MoS_2-based materials for high-performance LIBs anodes mainly involve in two strategies: (1) reducing the characteristic dimensions of MoS_2 and controlling the morphologies such as nanoflowers,[23] nanoflakes,[24] nanospheres,[25,26] and nanosheets;[27] and (2) building conductive and robust scaffold to improve both the kinetics and integrity,[28–33] such as embedding the single-layered MoS_2 in carbon nanofibers,[34] confining few-layered MoS_2 within 3D carbon nanosheets,[35] and coupling MoS_2 nanocrystals on N-enriched graphene[36] or N-doped carbon nanoboxes.[37] Although improved performance can be achieved, the development of novel highly stable MoS_2-based materials with fast kinetics remains challenging, owing to the lack of a ration design from molecular level. Moreover, it is also critical to correlate the performance with materials structure, and to understand the chemistry behind before its future practical applications.

Herein, we demonstrate a facile solvothermal synthesis of nanocomposites consisting few-layered MoS_2 and covalently sulfur-doped graphene (MoS_2/SG) with excellent electrochemical performance. We focus on not only the development of MoS_2-based electrode materials but also the materials design based on both structure and chemistry considerations. As shown in **Scheme 1**, the sulfur atoms covalently bonded to graphene sheets and effectively bridging 2D few-layered MoS_2 and graphene enable high robustness of the composite materials. Moreover, the intimate contact of MoS_2 and highly conductive graphene provides efficient electron transfer pathways, while the high surface of assembled 2D structured materials allows fast access to active materials. Such a unique composite architecture derived from the "bridging effect" ensures the electrode with an exceptional cycling stability and superior rate capability, which is also interpreted by the density functional theory (DFT) calculations. A capacity retention of 92.3% can be achieved after 2000 cycles at a current density of 10 A g^{-1}; even at a high current density of 20 A g^{-1}, the electrode still possesses a specific capacity of 766 mA h g^{-1}. This composite material with excellent electrochemical properties synthesized via a facile solvothermal approach holds great promise in the practical application of high-performance LIBs.

The MoS_2/SG composites were synthesized through a facile solvothermal approach with element sulfur as the precursor for both MoS_2 and S dopants of graphene, followed by annealing. X-ray diffraction (XRD) pattern of as-synthesized composites aligns well with literatures (JCPDS No. 77-1716)[38] with no obvious S peaks that can be found (Figure S1, Supporting Information), which can be indexed to a hexagonal crystal structure of MoS_2.[39] **Figure 1**A shows the representative

Dr. X. Wang, Dr. G. Li, Dr. M. H. Seo, F. M. Hassan, M. A. Hoque, Prof. Z. Chen
Department of Chemical Engineering
University of Waterloo
200 University Avenue West
Waterloo, Ontario N2L3G1, Canada
E-mail: zhwchen@uwaterloo.ca

DOI: 10.1002/aenm.201501106

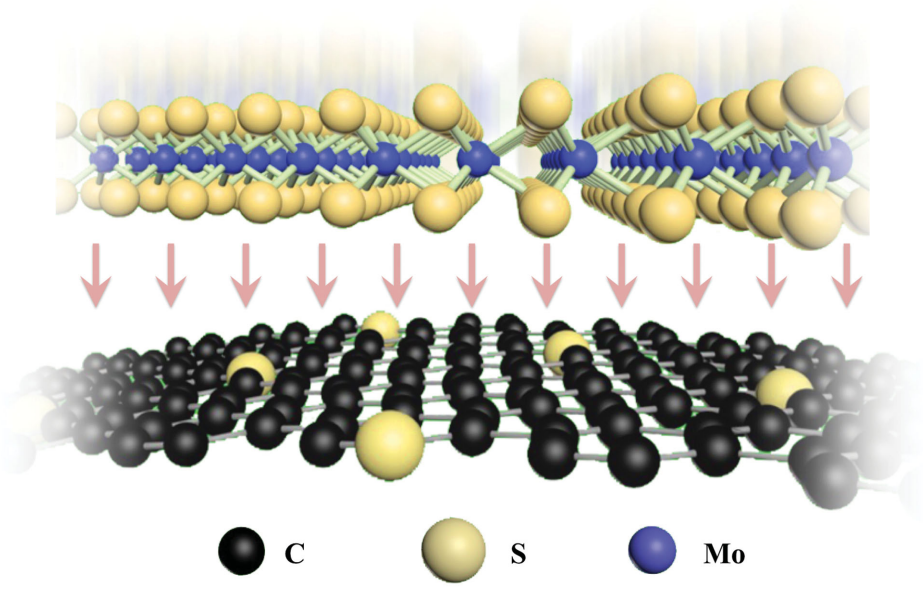

Scheme 1. The schematic of MoS_2/SG composites. The sulfur atoms are covalently bonded to graphene sheet, effectively bridging MoS_2 and graphene sheets.

scanning electron microscopy (SEM) image of as-synthesized composites. The composites exhibit a large-scale 2D sheet-like morphology with rough surface, implying the formation of MoS_2 on the surface of graphene, which is different from the pure MoS_2 synthesized at identical condition without graphene (Figure S2, Supporting Information) and other MoS_2/graphene materials obtained from hydrothermal synthesis with a flower-like or spherical morphology.[23,26] Figure 1B

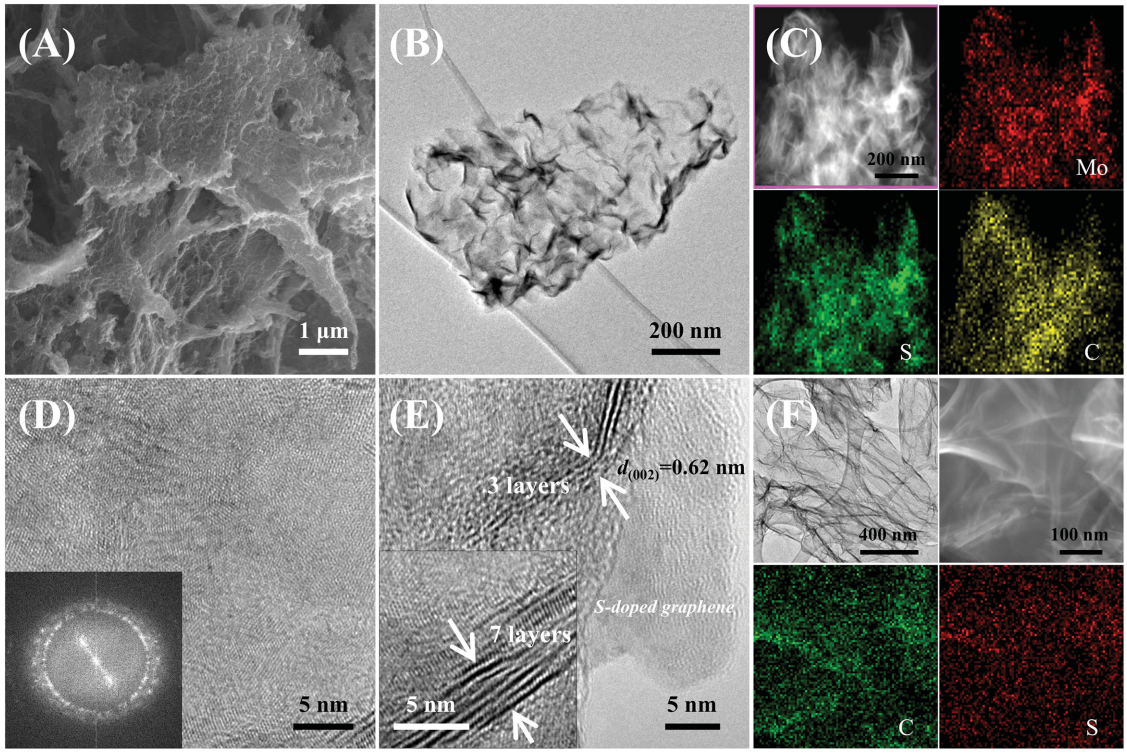

Figure 1. A) SEM and B) TEM images of as-synthesized MoS_2/SG composites; C) elemental mapping showing the distribution of MoS_2 and SG (up-left: spectrum image scanning, up-right: Mo-K mapping, bottom-left: S-K mapping, bottom-right: C-K mapping); D,E) high-resolution TEM images of as-synthesized MoS_2/SG composites (inset of (D): TEM FFT diffraction pattern); F) TEM image and elemental mapping of SG (top left: TEM image; top right: STEM image; bottom left: C-K mapping; bottom right: S-K mapping).

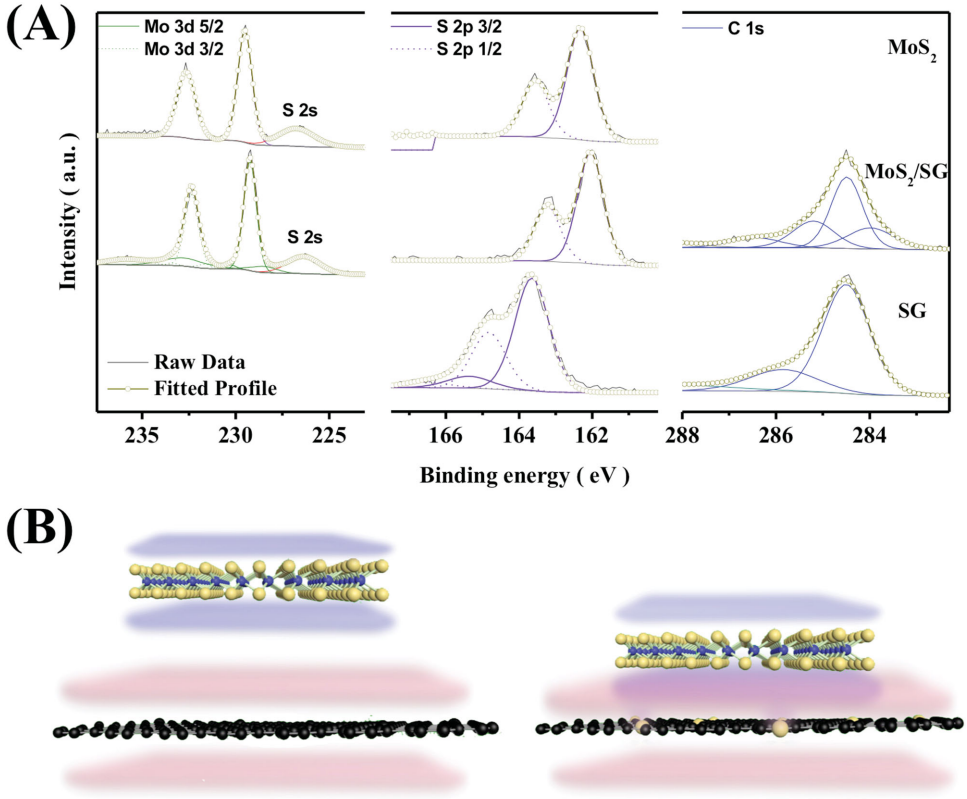

Figure 2. A) Chemical composition analysis by XPS for Mo, S, and C; and B) illustration of the strong interaction between MoS_2 and SG mainly stemming from the bridging effect of the S atoms doped in the graphene sheets.

presents the representative transmission electron microscopy (TEM) image of a single piece of as-synthesized composites. A silk veil-like structure with transparency can be observed, suggesting MoS_2 homogeneously distributed on graphene sheets, and both graphene and MoS_2 possess only a few layers. Such composites possess a surface area of 79 m^2 g^{-1}, which is lower than the graphene-based material synthesized at identical condition without using Mo precursor (Figure S3, Supporting Information), implying the formation of MoS_2 on the surface of graphene-based materials. To determine the constitution of the composites, energy-dispersive X-ray spectroscopy (EDS) was performed. The presence of elements Mo, S, and C confirms the formation of MoS_2 with graphene. Figure 1C shows the EDS elemental mapping of an area of the composites with uniform Mo, S, and C dispersion. This phenomenon further confirms that the MoS_2 is homogeneously distributed on graphene sheets. Moreover, two peaks located at 382.5 and 406.4 cm^{-1} can be found from the Raman spectrum of the composites (Figure S4, Supporting Information), corresponding to the typical vibrations of Mo–S atoms and suggesting the formation of few-layered MoS_2.[40,41] Figure 1D displays the high-resolution TEM image of the composites. It can be clearly observed that the MoS_2 is highly crystalline with a hexagonal arrangement, which agrees well with XRD result. The intrinsic layered structure analogous to graphene facilitates the epitaxial growth of MoS_2 over the graphene sheets, forming large continuous sheets. Interestingly, there are only a few (<10) layers, with an interlayer *d*-spacing of 0.62 nm (Figure 1E), which is consistent with Raman analysis and previous reports.[42] By comparison, S element still exists in the material synthesized at identical condition without using Mo precursor. As shown in Figure 1F, S uniformly disperses within graphene sheets, indicating the successful formation of S-doped graphene (SG). According to the thermogravimetric analysis (TGA, Figure S5, Supporting Information), the MoS_2 content in the composites is calculated to be ≈65.6%.

To analyze how S atoms interact with graphene sheets, X-ray photoelectron spectroscopy (XPS) was carried out on pure SG, pure MoS_2, and MoS_2/SG composite materials (Figure S6, Supporting Information). As shown in **Figure 2**A, the high-resolved XPS spectra of S in pure SG can be interpreted into two doublets. The two major peaks are located at 164.83 and 163.65 eV with a splitting energy of 1.18 V, confirming the presence of S atoms covalently bonded to graphene in a heterocyclic configuration.[43,44] Two minor peaks are observed at higher energy of 166.53 and 165.35 V, which could be attributed to a small amount of carbon bonded SO_x species.[45,46] In pure MoS_2, the binding energies of Mo $3d_{3/2}$ and $3d_{5/2}$, S $2p_{1/2}$ and $2p_{3/2}$ are 232.64 and 229.51 V, 163.55 and 162.37 V, respectively, showing the existence of Mo^{4+} and S^{2-}.[28] The stoichiometric ratio of S and Mo is estimated to be ≈2.08 based on the peak area, further indicating the formation of MoS_2. For the as-synthesized MoS_2/SG composites, two major peaks from Mo are centered at 232.36 and 229.23 V, while peaks from S are at 163.28 and 162.10 V. Compared to pure MoS_2, both Mo and S peaks show a slight shift to the lower energy regions,

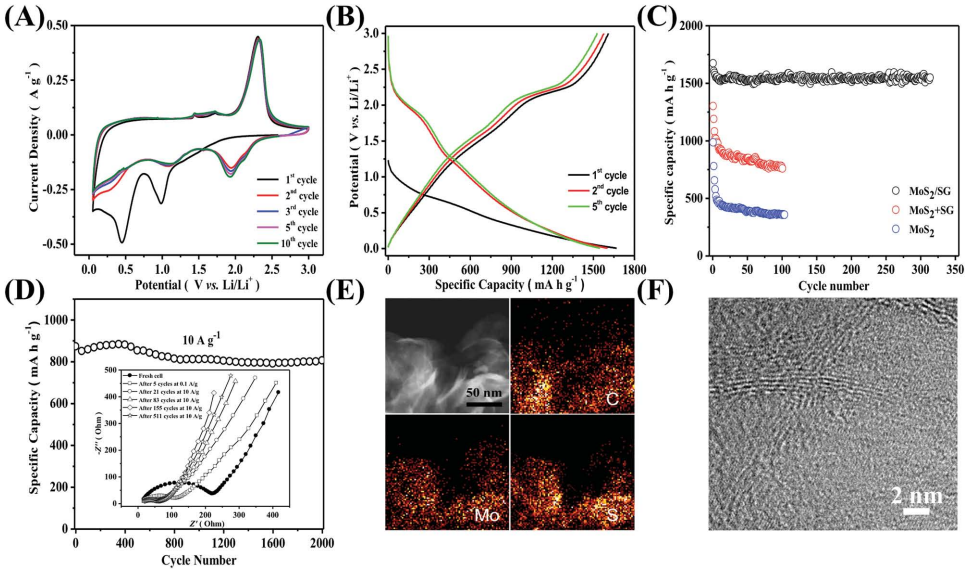

Figure 3. A) CV plots of a representative MoS_2/SG composite electrode at a sweep rate of 0.1 mV s^{-1} between 3.0 and 0.005 V; B) galvanostatic charge/discharge curves of a composite electrode at a current densities of 0.1 A g^{-1} between 3.0 and 0.005 V; C) Comparison of cycling stability of MoS_2/SG composites with pure MoS_2 and physically mixed MoS_2 and SG at a current density of 0.1 A g^{-1}; D) long-term cycling performance of MoS_2/SG composites at a high current density of 10 A g^{-1} (inset: the Nyquist plot of the composite electrode at frequencies from 100 kHz to 0.01 Hz at different cycling status); E) high-magnification HAADF-STEM image of MoS_2/SG composite after cycling test and the corresponding energy-dispersive X-ray spectroscopy (EDS) mapping of the elements C, Mo, and S; and F) high-resolution TEM images of as-synthesized MoS_2/SG composites after cycling test.

suggesting an increased density of electron clouds around few-layered MoS_2. Considering that chemically S doping makes graphene more electron-rich,[46] and that MoS_2 is a p-type semiconductor material,[30,47] the electron clouds bias to MoS_2 from SG, forming a strong electronic coupling between each other. Moreover, the peaks from the S dopants in SG disappear, indicating that the oxidation state of these S atoms decreases by sharing the electron clouds with MoS_2. Therefore, as illustrated in Figure 2B, the strong interaction between MoS_2 and SG is mainly stemmed from the bridging effect of the S atoms doped in the graphene sheets. This unique microstructure endows the MoS_2/SG composites with a highly stable structure for long-term cycling in LIBs applications.

The electrochemical performance of MoS_2/SG composites was tested using CR2032 coin cells where lithium foil was used for counter electrode and 1.0 M $LiPF_6$ in EC/DMC (v/v = 1:1) for electrolyte. **Figure 3**A shows the typical cyclic voltammograms of MoS_2/SG composites, where two strong cathodic peaks located at 0.99 and 0.45 V could be found for the initial cycle, corresponding to the Li^+ intercalation process forming Li_xMoS_2, and the further conversion to Mo embedded in Li_2S matrix, respectively. Two minor anodic peaks at 1.44 and 1.72 V followed by a strong peak at 2.30 V can be observed, which is mainly ascribed to the oxidation of Mo (from Mo^0 to Mo^{4+} and from Mo^{4+} to Mo^{6+} finally) and Li_2S, respectively. As expected, the MoS_2/SG composites show a good stability during scanning, since the cyclic voltammetric (CV) curves for the subsequent cycles are highly similar in both shape and size. The two cathodic peaks at 0.99 and 0.45 V disappeared, indicating the irreversible depletion of 2H-MoS_2. Instead, a strong peak at 1.94 V and a minor peak at 1.10 V arise, which can be coupled with anodic peaks, showing the reversible redox reactions. The excellent cycling stability can also be observed from the galvanostatic charge–discharge processes. As shown in Figure 3B, an initial discharge capacity of 1670 mA h g^{-1} can be achieved, with a high initial Coulombic efficiency of 96.5%. Two discharge plateaus at 2.0 and 1.2 V and two charge plateaus at 1.6 and 2.3 V can be found after initial discharge process, which is highly consistent with CV observations. The corresponding cycling performance is displayed in Figure 3C. After over 300 cycles at a constant current density of 0.1 A g^{-1}, the MoS_2/SG composites still possess a discharge capacity of 1546 mA h g^{-1}, which corresponds to 92.6% of its initial capacity, indicating a long cycling stability. By comparison, both pure MoS_2 synthesized at identical condition and physically mixed MoS_2 and graphene material show a dramatic capacity decay during cycling. This phenomenon suggests that the in situ growth and the S atoms in doped graphene play a critical role in bridging the MoS_2 and graphene sheets, enabling a robust architecture of the composites for long-term cycling. The superior cycling performance can be further revealed even at high current densities. As shown in Figure 3D, a discharge capacity retention of 92.3% can be achieved after 2000 cycles at a current density of 10 A g^{-1}. To the best of our knowledge, such an extraordinary cycling stability is firstly reported on MoS_2-based materials, and confirmed by the electrochemical impedance spectroscopy (EIS) where the small resistance and fast ion-diffusion are maintained during cycling. The robust composite architecture is further revealed by TEM images of the MoS_2/SG after cycling testing (Figure S7, Supporting Information). The high angle annular dark field scanning transmission electron microscopy (HAADF-STEM) image in Figure 3E confirms that the 2D layered structure of MoS_2 is preserved and combined well with SG sheets, while the MoS_2 is still highly crystalline with a few layers (Figure 3F).

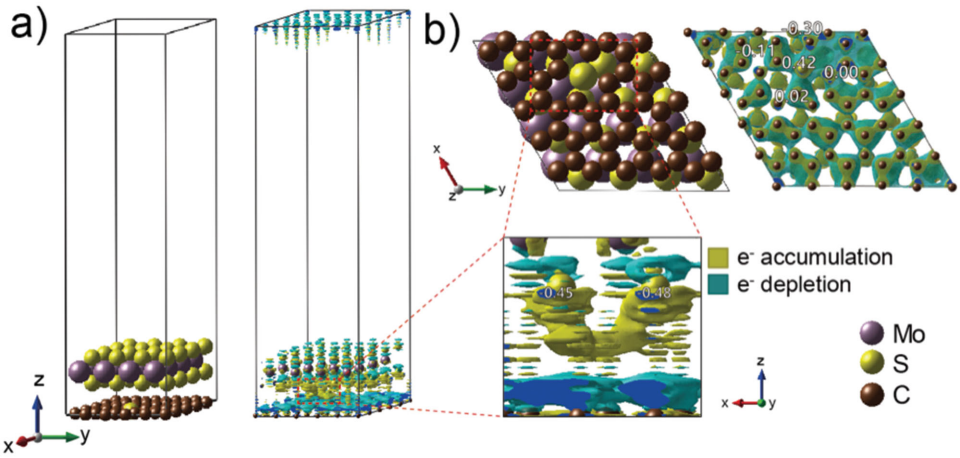

Figure 4. A) The side and B) the bottom view of relaxed MoS_2 on SG with charge density changes, and the corresponding Bader charges of S atoms from MoS_2 as well as C atoms and S dopant from SG.

To better understand this extraordinary cycling stability, we analyze the structure of the materials by calculating the binding energies based on density functional theory. The fully relaxed structure of bulk MoS_2 and projected density of states of Mo 3d orbital in the MoS_2 is shown in Figure S8 (Supporting Information). After stabilization, the lattice of the MoS_2 bulk was evaluated to be 3.18, 3.18, and 13.55 Å at the *x*-, *y*-, and *z*-axes, which is consistent with the previously reported experimental work.[48] Note that the formation of thiophene-like structure is more favourable during the SG synthesis since the formation energy is lower than that of graphitic structured SG.[49] We designed the (4 × 4) MoS_2 monolayer on a (5 × 5) thiophene like SG, imposing a commensurability condition between the SG and MoS_2 monolayer. To define thermodynamically stable MoS_2 on SG, 75 configurations of different S location in the lattice of SG have been generated. Among them, the structure shown in **Figure 4** has been chosen since it has the lowest ground state energy. The adsorption energy (ΔE_{ads}) of MoS_2 on SG surface was calculated according to the following equation

$$\Delta E_{ads} = E_{MOS2\text{-}SG} - E_{MOS2} - E_{SG} \quad (1)$$

where $E_{MoS2\text{-}SG}$, E_{MoS2}, and E_{SG} are total energies of MoS_2 deposited SG, the monolayer of MoS_2, and an SG model, respectively. Interestingly, the MoS_2 monolayer adsorption energy on the SG was calculated to be only +1.08 eV without considering the van der Waals interaction, suggesting that the SG is not energetically desirable for MoS_2. This result is conflicting with the XPS observation and other reported work including MoS_2/graphene,[50] MoS_2/N-doped graphene.[30] Therefore, the binding of MoS_2 on the substrate could be happened via other mechanisms such as van der Waals interaction and electrostatic. Note that it is reported that the considerably negligible adsorption of MoS_2 is arisen on graphene.[51] With van der Waals correction by DFT-D2 method of Grimme,[52,53] the adsorption energy of a monolayer of MoS_2 was evaluated to be −1.37 eV, revealing the spontaneous adsorption occurring on SG, which is consistent with the XPS observation and strongly supports the highly stable cycling performance.

The physicochemical and electronic interaction between MoS_2 and SG, which is determined by its electronic structure in valence electrons,[54–60] plays an imperative role in the stability. To further understand the interaction derived from the shared electron clouds, the charge density changes, $\Delta\rho$, was investigated according to following equation

$$\Delta\rho = \rho_{MOS2\text{-}SG} - \rho_{MOS2} - \rho_{SG} \quad (2)$$

where $\rho_{MoS2\text{-}SG}$, ρ_{MoS2}, and ρ_{SG} are the charge densities of MoS_2/SG, MoS_2, and SG, respectively. Moreover, Bader change analysis[61] which calculates the charge of an individual atom in model system[49,62] was also conducted on the MoS_2/SG system to understand the movement of an amount of charge. As shown in Figure 4, the charge of S dopant is depleted to be 0.48e for SG in MoS_2/SG, whereas the nearest three S atoms from MoS_2 get charges of –0.45, –0.45, and –0.48e, respectively. Therefore, there is a meaningful amount of charge transfer from SG to MoS_2, which negatively polarizes the interface between MoS_2 and SG. This result is consistent with the XPS analysis, where the electronic interaction between MoS_2 with SG leads to the robust composite architecture.

In addition to the exceptional cycling stability, the bridging effect of S dopants ensures the intimate contact between active MoS_2 and highly conductive graphene sheets, which enables a significantly improved rate capability. As shown in **Figure 5**A, the MoS_2/SG composites deliver a specific capacity of 1672, 1398, 1324, 1228, 1137 mA h g^{-1} at a current density of 0.1, 0.2, 0.5, 1.0, 2.0 A g^{-1}. The corresponding capacity dependence on current density is presented in Figure 5B. Even at a current density of 10 and 20 A g^{-1}, a specific capacity of 915 and 766 mA h g^{-1} can be obtained, which is equal to a capacity retention of 64.8% and 54.1%, respectively. Impressively, the MoS_2/SG composites still possess a discharge and charge capacity of 522 mA h g^{-1} at 50 A g^{-1}, with a discharging and charging time of 37 s. The composite materials with such a capacitive behavior outperforms most of the other MoS_2-based composite materials (Figure 5C),[34,39,63–67] which makes it highly promising in future applications of electric transportation. Remarkably, the robustness of the composite architecture can be further

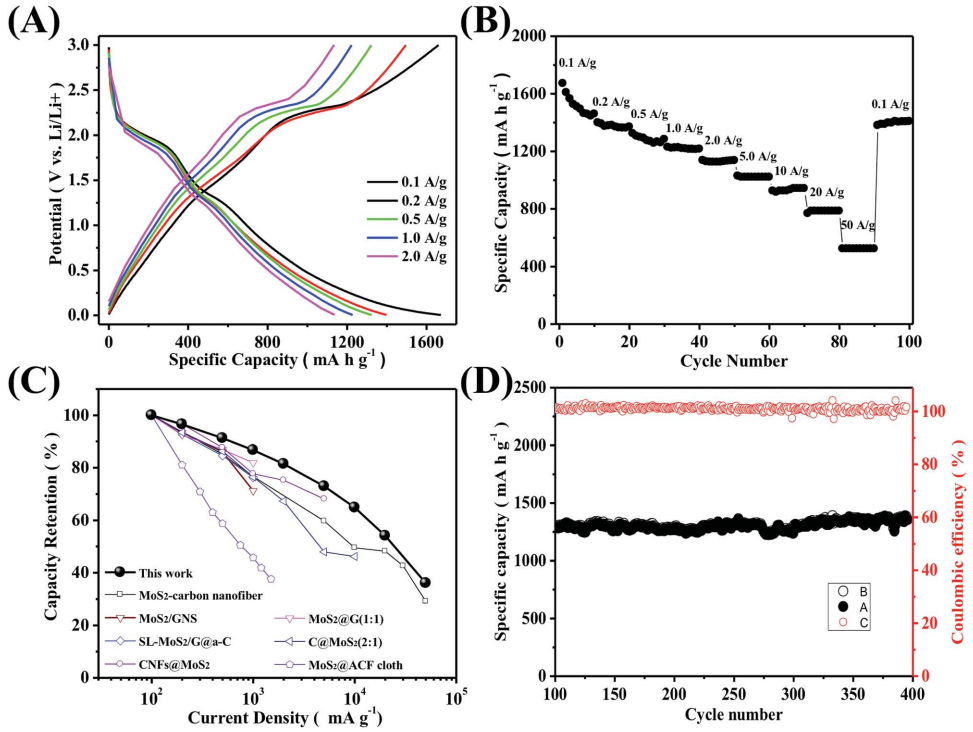

Figure 5. A) Galvanostatic charge/discharge curves of a composite electrode at various current densities from 0.1 to 50 A g^{-1} between 3.0 and 0.005 V; B) corresponding rate performance of the composite electrode; C) comparison of the rate capability of MoS_2/SG composites with various MoS_2-based high-rate electrodes reported recently[34,39,63–67] (the capacitance was normalized by specific capacitance at the current density of 0.1 mA g^{-1}); and D) cycling performance of the electrode at a current density of 0.1 A g^{-1} for another 300 cycles after rate capability testing.

observed after the rate performance testing. A specific capacity of 1379 mA h g^{-1} can be recovered at a current density of 0.1 A g^{-1}. Moreover, the electrode was cycled for another 300 cycles at a current of 0.1 A g^{-1} (Figure 5D). The capacity still can be stabilized, and even shows a gradual increase with a high Coulombic efficiency. This phenomenon is mainly attributed to the increased number of defect sites and vacancies on graphene sheets, which has been reported previously.[30]

In summary, we have successfully developed a novel composite material based on MoS_2 and SG for high-performance LIBs anode. Both experimental and computational investigations confirm that the sulfur atoms are successfully bonded to graphene covalently, and efficiently bridge the layered MoS_2 and graphene sheets by sharing electron clouds, resulting in a robust composite architecture. Such a composite exhibits a remarkably long cycling stability (92.3% capacity retention for 2000 cycles at a current density of 10 A g^{-1}) and a superior rate capability (1672 and 915 mA h g^{-1} at 0.1 and 10 A g^{-1}, respectively). We believe this design, the facile and scalable synthesis can be extended to other materials, and these composite materials hold great promise in next-generation rechargeable LIBs.

Experimental Section

Synthesis of MoS_2/SG Composites: Graphene oxide (GO) was prepared from powdered flake graphite (400 mesh) by a modified Hummers method as described previously.[68] MoS_2/SG composites were synthesized via a facial one-pot solvothermal method. In a typical synthesis, GO (30 mg) was dispersed in ethylene glycol (10 mL) by ultrasonication for 1 h. Aqueous solutions of sodium molybdate dehydrate (100 mg mL^{-1}, 2 mL) and thiourea (200 mg mL^{-1}, 1 mL) were added into GO solution, respectively. Elemental sulfur (20 mg) was then added before the solution was transferred into a polytetrafluoroethylene (PTFE)-lined 20 mL capacity stainless steel autoclave and kept at 120 °C for 10 h followed by 220 °C for another 10 h. The precipitate was collected by filtration and washed with water and ethanol followed by freeze-drying for 2 d. The black and fluffy power was annealed at 800 °C for 6 h under Argon flow with a ramping rate of 2 °C min^{-1}. Pure MoS_2 and pure SG were synthesized at identical conditions.

Materials Characterization: The crystal structures of the as-prepared materials were characterized by XRD (X'Pert Pro X-ray diffractometer, Panalytical B.V.). The morphology and composition of the materials were examined using scanning electron microscopy (SEM, LEO FESEM 1530) and TEM (JEOL 2010F TEM/STEM field emission microscope) equipped with a large solid angle for high-X-ray throughput, scanning, scanning-transmission and a Gatan imaging filter (GIF) for energy filtered imaging from the Canadian Center for Electron Microscopy (CCEM) located at McMaster University. TGA was conducted on TA instrument Q500. TGA testing was performed in air with a temperature range of 25 to 850 °C and a ramp rate of 10 °C min^{-1}. Nitrogen sorption isotherms were measured at 77 K with a Micromeritics ASAP 2020 analyzer. The samples were degassed in vacuum at 200 °C for 3 h. The specific surface areas were calculated by the Brunauer–Emmett–Teller (BET) method using adsorption branch in a relative pressure range from 0.04 to 0.25. The pore size distributions were derived from the adsorption branches of isotherms using the Barrett–Joyner–Halenda (BJH) model. X-ray photoelectron spectra were collected by XPS (Thermal Scientific *K*-Alpha XPS spectrometer). Raman scattering spectra were recorded on a Bruker Sentterra system (532 nm laser).

Electrode Fabrication: A convention slurry-coating process was used to fabricate the electrodes. The active material powders, Super P conductive

agent and poly(vinylidene fluoride) (PVDF) binder were mixed in a mass ratio of 80:10:10, and homogenized in *N*-Methyl-2-pyrrolidone (NMP) to form slurries. The homogenous slurries were uniformly coated on Cu foil substrates and dried at 100 °C for 12 h under vacuum. As-formed electrodes were then pressed at a pressure of 2.0 MPa. The mass loading on each electrode was controlled to be ≈1.5 mg cm^{-2}.

Electrochemical Measurements: To test electrodes, 2032-type coin cells were assembled in an argon-filled glovebox, using Celgard 2500 membrane as the separator, lithium foils as the counter electrodes, 1 M $LiPF_6$ in a 1:1 (v/v) mixture of ethylene carbonate and dimethyl carbonate as the electrolyte. CV measurements were carried out on a VMP3 potentiostat/galvanostat (Bio-Logic LLC, Knoxville, TN) using cutoff voltages of 3.0 and 0.005 V versus Li/Li^+ at different scan rates. The galvanostatic charge/discharge measurements were performed on NEWARE BTS-CT3008 (Neware Technology, Ltd., Shenzhen, China) at different current densities. EIS measurement was conducted on a Princeton Applied Research VersaSTAT MC potentiostat. The Nyquist plots were recorded potentiostatically by applying an AC voltage of 10 mV amplitude in the frequency range of 0.01 to 10^5 Hz. All electrochemical measurements were carried out at room temperature.

Computational: The Vienna *ab* initio simulation package program was employed to find the ground state energy of MoS_2 and MoS_2 on SG model with the implemented DFT method.[69–71] The Perdew, Burke, and Ernzerhof (PBE) functional defined the electron exchange-correlation energy,[72] taking on the spin-polarized generalized gradient approximation.[73,74] The valence electrons were described by Kohn-Sham wave functions, which were expanded with a plane-wave basis set. The core electrons were replaced by projector augmented wave pseudo-potentials.[75,76] A cutoff energy of 520 eV was used. All ions were fully relaxed during the structural optimization until the total energy was converged within 10^{-4} eV. A gamma point mesh with ($15 \times 15 \times 15$) *k* points was used for the graphene (1×1) unit cell to sample the Brillouin zone for bulk calculation. The thiophene-like SG sheets having (5×5) supercells as described by our previous literature[49] are fully relaxed to optimize the structures with (4×4) MoS_2 monolayer deposited on the supports. To calculate the total energies of MoS_2 on SG model, we only used a gamma point mesh of ($5 \times 5 \times 1$), and utilized the Methfessel–Paxton smearing method[77] as well as the van der Waals corrections conducted by DFT-D2 method of Grimme.[52,53]

Supporting Information

Supporting Information is available from the Wiley Online Library or from the author.

Acknowledgements

X.W. and G.L. contributed equally to this work. This work was supported by the Natural Sciences and Engineering Research Council of Canada (NSERC), University of Waterloo, and the Waterloo Institute for Nanotechnology. The authors acknowledge Dr. Carmen Andrei and Canadian Centre for Electron Microscopy at McMaster University for TEM characterization.

Received: June 4, 2015
Revised: July 22, 2015
Published online: September 22, 2015

[1] M. Armand, J. M. Tarascon, *Nature* **2008**, *451*, 652.
[2] N. Armaroli, V. Balzani, *Energy Environ. Sci.* **2011**, *4*, 3193.
[3] B. Dunn, H. Kamath, J.-M. Tarascon, *Science* **2011**, *334*, 928.
[4] P. G. Bruce, B. Scrosati, J.-M. Tarascon, *Angew. Chem. Int. Ed.* **2008**, *47*, 2930.
[5] M. S. Whittingham, *Chem. Rev.* **2004**, *104*, 4271.
[6] J. R. Dahn, T. Zheng, Y. Liu, J. S. Xue, *Science* **1995**, *270*, 590.
[7] M. S. Whittingham, *MRS Bull.* **2008**, *33*, 411.
[8] A. Manthiram, *J. Phy. Chem. Lett.* **2011**, *2*, 176.
[9] A. S. Arico, P. Bruce, B. Scrosati, J.-M. Tarascon, W. van Schalkwijk, *Nat. Mater.* **2005**, *4*, 366.
[10] L. Ji, Z. Lin, M. Alcoutlabi, X. Zhang, *Energy Environ. Sci.* **2011**, *4*, 2682.
[11] M. T. McDowell, S. W. Lee, W. D. Nix, Y. Cui, *Adv. Mater.* **2013**, *25*, 4966.
[12] C. K. Chan, H. Peng, G. Liu, K. Mcilwrath, X. F. Zhang, R. A. Huggins, Y. Cui, *Nat. Nanotechnol.* **2008**, *3*, 31.
[13] K. T. Lee, Y. S. Jung, S. M. Oh, *J. Am. Chem. Soc.* **2003**, *125*, 5652.
[14] P. Poizot, S. Laruelle, S. Grugeon, L. Dupont, J. M. Tarascon, *Nature* **2000**, *407*, 496.
[15] L. Zhao, Y.-S. Hu, H. Li, Z. Wang, L. Chen, *Adv. Mater.* **2011**, *23*, 1385.
[16] H.-G. Jung, S.-T. Myung, C. S. Yoon, S.-B. Son, K. H. Oh, K. Amine, B. Scrosati, Y.-K. Sun, *Energy Environ. Sci.* **2011**, *4*, 1345.
[17] M. Noh, Y. Kwon, H. Lee, J. Cho, Y. Kim, M. G. Kim, *Chem. Mater.* **2005**, *17*, 1926.
[18] X. Lou, C. Yuan, L. Archer, *Adv. Mater.* **2007**, *19*, 3328.
[19] J. Jiang, Y. Li, J. Liu, X. Huang, C. Yuan, X. W. Lou, *Adv. Mater.* **2012**, *24*, 5166.
[20] M. Chhowalla, H. S. Shin, G. Eda, L.-J. Li, K. P. Loh, H. Zhang, *Nat. Chem.* **2013**, *5*, 263.
[21] J. Xiao, D. Choi, L. Cosimbescu, P. Koech, J. Liu, J. P. Lemmon, *Chem. Mater.* **2010**, *22*, 4522.
[22] C. Feng, J. Ma, H. Li, R. Zeng, Z. Guo, H. Liu, *Mater. Res. Bull.* **2009**, *44*, 1811.
[23] Z. Hu, L. Wang, K. Zhang, J. Wang, F. Cheng, Z. Tao, J. Chen, *Angew. Chem.* **2014**, *126*, 13008.
[24] H. Hwang, H. Kim, J. Cho, *Nano Lett.* **2011**, *11*, 4826.
[25] S.-K. Park, S.-H. Yu, S. Woo, J. Ha, J. Shin, Y.-E. Sung, Y. Piao, *CrystEngComm* **2012**, *14*, 8323.
[26] S. Ding, D. Zhang, J. S. Chen, X. W. Lou, *Nanoscale* **2012**, *4*, 95.
[27] S. Ding, J. S. Chen, X. W. Lou, *Chem.-Eur. J.* **2011**, *17*, 13142.
[28] Y. Shi, Y. Wang, J. I. Wong, A. Y. S. Tan, C.-L. Hsu, L.-J. Li, Y.-C. Lu, H. Y. Yang, *Sci. Rep.* **2013**, *3*, 2169.
[29] Y. Wang, G. Xing, Z. J. Han, Y. Shi, J. I. Wong, Z. X. Huang, K. Ostrikov, H. Y. Yang, *Nanoscale* **2014**, *6*, 8884.
[30] K. Chang, D. Geng, X. Li, J. Yang, Y. Tang, M. Cai, R. Li, X. Sun, *Adv. Energy Mater.* **2013**, *3*, 839.
[31] Y. Gong, S. Yang, Z. Liu, L. Ma, R. Vajtai, P. M. Ajayan, *Adv. Mater.* **2013**, *25*, 3979.
[32] L. Yang, S. Wang, J. Mao, J. Deng, Q. Gao, Y. Tang, O. G. Schmidt, *Adv. Mater.* **2013**, *25*, 1180.
[33] C. Zhang, Z. Wang, Z. Guo, X. W. Lou, *ACS Appl. Mater. Interfaces* **2012**, *4*, 3765.
[34] C. Zhu, X. Mu, P. A. van Aken, Y. Yu, J. Maier, *Angew. Chem. Int. Ed.* **2014**, *53*, 2152.
[35] J. Zhou, J. Qin, X. Zhang, C. Shi, E. Liu, J. Li, N. Zhao, C. He, *ACS Nano* **2015**, *9*, 3837.
[36] Y. Tang, D. Wu, Y. Mai, H. Pan, J. Cao, C. Yang, F. Zhang, X. Feng, *Nanoscale* **2014**, *6*, 14679.
[37] X.-Y. Yu, H. Hu, Y. Wang, H. Chen, X. W. Lou, *Angew. Chem. Int. Ed.* **2015**, *54*, 7395.
[38] X. L. Li, Y. D. Li, *Chem.-Eur. J.* **2003**, *9*, 2726.
[39] K. Chang, W. Chen, *ACS Nano* **2011**, *5*, 4720.
[40] H. Li, Q. Zhang, C. C. R. Yap, B. K. Tay, T. H. T. Edwin, A. Olivier, D. Baillargeat, *Adv. Funct. Mater.* **2012**, *22*, 1385.
[41] Y. Hu, X. Li, A. Lushington, M. Cai, D. Geng, M. N. Banis, R. Li, X. Sun, *ECS J. Solid State SC* **2013**, *2*, M3034.

[42] Y. Feldman, E. Wasserman, D. J. Srolovitz, R. Tenne, *Science* **1995**, *267*, 222.
[43] Z. Yang, Z. Yao, G. Li, G. Fang, H. Nie, Z. Liu, X. Zhou, X. A. Chen, S. Huang, *ACS Nano* **2012**, *6*, 205.
[44] B. Quan, S.-H. Yu, D. Y. Chung, A. Jin, J. H. Park, Y.-E. Sung, Y. Piao, *Sci. Rep.* **2014**, *4*.
[45] Z. Ma, S. Dou, A. Shen, L. Tao, L. Dai, S. Wang, *Angew. Chem. Int. Ed.* **2015**, *54*, 1888.
[46] D. Higgins, M. A. Hoque, M. H. Seo, R. Wang, F. Hassan, J.-Y. Choi, M. Pritzker, A. Yu, J. Zhang, Z. Chen, *Adv. Funct. Mater.* **2014**, *24*, 4325.
[47] F. Meng, J. Li, S. K. Cushing, M. Zhi, N. Wu, *J. Am. Chem. Soc.* **2013**, *135*, 10286.
[48] K. K. Liu, W. J. Zhang, Y. H. Lee, Y. C. Lin, M. T. Chang, C. Su, C. S. Chang, H. Li, Y. M. Shi, H. Zhang, C. S. Lai, L. J. Li, *Nano Lett.* **2012**, *12*, 1538.
[49] D. Higgins, M. A. Hoque, M. H. Seo, R. Wang, F. Hassan, J.-Y. Choi, M. Pritzker, A. Yu, J. Zhang, Z. Chen, *Adv. Funct. Mater.* **2014**, *24*, 4325.
[50] J. Xiao, X. Wang, X.-Q. Yang, S. Xun, G. Liu, P. K. Koech, J. Liu, J. P. Lemmon, *Adv. Funct. Mater.* **2011**, *21*, 2840.
[51] Y. D. Ma, Y. Dai, M. Guo, C. W. Niu, B. B. Huang, *Nanoscale* **2011**, *3*, 3883.
[52] J. P. Perdew, K. Burke, M. Ernzerhof, *Phy. Rev. Lett.* **1997**, *78*, 1396.
[53] S. Grimme, *J. Comput. Chem.* **2006**, *27*, 1787.
[54] M. H. Seo, H. W. Park, D. U. Lee, M. G. Park, Z. Chen, *ACS Catal.* **2015**, *5*, 4337.
[55] B. I. Lundqvist, O. Gunnarsson, H. Hjelmberg, J. K. Norskov, *Surf. Sci.* **1979**, *89*, 196.
[56] B. Hammer, J. K. Norskov, *Nature* **1995**, *376*, 238.
[57] B. Hammer, J. K. Nørskov, *Adv. Catal.* **2000**, *45*, 71.
[58] F. Calle-Vallejo, O. A. Díaz-Morales, M. J. Kolb, M. T. M. Koper, *ACS Catal.* **2015**, *5*, 869.
[59] F. Calle-Vallejo, J. I. Martinez, J. M. Garcia-Lastra, M. Mogensen, J. Rossmeisl, *Angew. Chem. Int. Ed.* **2010**, *49*, 7699.
[60] F. Calle-Vallejo, N. G. Inoglu, H. Y. Su, J. I. Martınez, I. C. Man, M. T. M. Koper, J. R. Kitchin, J. Rossmeisl, *Chem. Sci.* **2013**, *4*, 1245.
[61] R. F. W. Bader, *Atoms in Molecules: A Quantum Theory*, Oxford University Press, New York **1994**.
[62] M. H. Seo, S. M. Choi, E. J. Lim, I. H. Kwon, J. K. Seo, S. H. Noh, W. B. Kim, B. Han, *ChemSusChem* **2014**, *7*, 2609.
[63] K. Chang, W. Chen, *Chem. Commun.* **2011**, *47*, 4252.
[64] K. Chang, W. Chen, *J. Mater. Chem.* **2011**, *21*, 17175.
[65] S. Hu, W. Chen, J. Zhou, F. Yin, E. Uchaker, Q. Zhang, G. Cao, *J. Mater. Chem. A* **2014**, *2*, 7862.
[66] F. Zhou, S. Xin, H.-W. Liang, L.-T. Song, S.-H. Yu, *Angew. Chem. Int. Ed.* **2014**, *53*, 11552.
[67] C. Wang, W. Wan, Y. Huang, J. Chen, H. H. Zhou, X. X. Zhang, *Nanoscale* **2014**, *6*, 5351.
[68] D. Li, M. B. Muller, S. Gilje, R. B. Kaner, G. G. Wallace, *Nat. Nanotechnol.* **2008**, *3*, 101.
[69] G. Kresse, J. Furthmüller, *Phys. Rev. B* **1996**, *54*, 11169.
[70] P. Hohenberg, W. Kohn, *Phys. Rev.* **1964**, *136*, B864.
[71] W. Kohn, L. J. Sham, *Phys. Rev. A* **1965**, *140*, 1133.
[72] J. P. Perdew, K. Burke, M. Ernzerhof, *Phys. Rev. Lett.* **1996**, *77*, 3865.
[73] G. Kresse, J. Furthmuller, *Comput. Mater. Sci.* **1996**, *6*, 15.
[74] J. P. Perdew, K. Burke, Y. Wang, *Phy. Rev. B* **1996**, *54*, 16533.
[75] G. Kresse, D. Joubert, *Phys. Rev. B* **1999**, *59*, 1758
[76] P. E. Blöchl, *Phys. Rev. B* **1994**, *50*, 17953.
[77] M. Methfessel, A. T. Paxton, *Phys. Rev. B* **1989**, *40*, 3616.